CrossMark

GASTROINTESTINAL

Prediction of pancreatic neuroendocrine tumour grade with MR imaging features: added value of diffusion-weighted imaging

Emad Lotfalizadeh[1] · Maxime Ronot[1,2,3] · Mathilde Wagner[1,3] · Jérôme Cros[2,4] ·
Anne Couvelard[2,4] · Marie-Pierre Vullierme[1] · Wassim Allaham[1] · Olivia Hentic[5] ·
Philippe Ruzniewski[5] · Valérie Vilgrain[1,2,3]

Abstract

Objectives To evaluate the value of MR imaging including diffusion-weighted imaging (DWI) for the grading of pancreatic neuroendocrine tumours (pNET).

Material and Methods Between 2006 and 2014, all resected pNETs with preoperative MR imaging including DWI were included. Tumour grading was based on the 2010 WHO classification. MR imaging features included size, T1-w, and T2-w signal intensity, enhancement pattern, apparent (ADC) and true diffusion (D) coefficients.

Results One hundred and eight pNETs (mean 40 ± 33 mm) were evaluated in 94 patients (48 women, 51 %, mean age 52 ± 12). Fifty-five (51 %), 42 (39 %), and 11 (10 %) tumours were given the following grades (G): G1, G2, and G3. Mean ADC and D values were significantly lower as grade increased (ADC: 2.13 ± 0.70, 1.78 ± 0.72, and 0.86 ± 0.22 10^{-3} mm^2/s,

and D: 1.92 ± 0.70, 1.75 ± 0.74, and 0.82 ± 0.19 10^{-3} mm^2/s G1, G2, and G3, all $p < 0.001$). A higher grade was associated with larger sized tumours ($p < 0.001$). The AUROC of ADC and D to differentiate G3 and G1-2 were 0.96 ± 0.02 and 0.95 ± 0.02. Optimal cut-off values for the identification of G3 were 1.19 10^{-3} mm^2/s for ADC (sensitivity 100 %, specificity 92 %) and 1.04 10^{-3} mm^2/s for D (sensitivity 82 %, specificity 92 %).

Conclusion Morphological/functional MRI features of pNETS depend on tumour grade. DWI is useful for the identification of high-grade tumours.

Key Points
• *Morphological and functional MRI features of pNETs depend on tumour grade.*
• *Their combination has a high predictive value for grade.*
• *All pNETs should be explored by MR imaging including DWI.*
• *DWI is helpful for identification of high-grade and poorly-differentiated tumours.*

✉ Maxime Ronot
  maxime.ronot@bjn.aphp.fr

[1] Department of Radiology, University Hospitals Paris Nord Val de Seine, Beaujon, Clichy, Hauts-de-Seine, France

[2] University Paris Diderot, Sorbonne Paris Cité, Paris, France

[3] INSERM U1149, Centre de Recherche Biomédicale Bichat-Beaujon, CRB3, Paris, France

[4] Department of Pathology, University Hospitals Paris Nord Val de Seine, Beaujon, Clichy, Hauts-de-Seine, France

[5] Department of Gastroenterology, University Hospitals Paris Nord Val de Seine, Beaujon, Clichy, Hauts-de-Seine, France

Keywords Neoplasm · Pancreas · Ki-67 · Carcinoma · Grading

Abbreviations
ADC	apparent diffusion coefficient
D	true diffusion coefficient
DWI	diffusion-weighted imaging
ENETS	European Neuroendocrine Tumour Society
G	grade
(p)NET	(pancreatic) neuroendocrine tumour
MRI	magnetic resonance imaging
WHO	World Health Organization

Introduction

Pancreatic neuroendocrine tumours (pNETs) are uncommon neoplasms with an estimated incidence of less than 1 per 100,000 per year in the general population [1]. Nevertheless, the incidence and prevalence of this entity has increased in the last decade [2].

One of the most important factors in the management of pNETS is tumour grade assessed by the Ki67 index, which corresponds to the percentage of tumour cells whose nucleus is marked by the monoclonal antibody MIB-1. According to the European Neuroendocrine Tumour Society (ENETS) and the 2010 revised World Health Organization (WHO) recommendations [3, 4], pNETs are classified according to their Ki67 index. Grade 1 (G1) corresponds to tumours ≤2 % Ki67 index, grade 2 (G2) to lesions 3–20 % Ki67 index, and grade 3 (G3) to tumours >20 % Ki67 index. This grading system is strongly correlated to survival, with 5-year survival rates ranging from 60–100 % for G1 and G2 tumours to 29 % for G3 carcinomas [5]. Recently, these cut-off values have become a subject of debate, and authors have suggested that 5 % or 10 % cut-off values may be more clinically significant than 2 % and 20 % [1, 6, 7].

Well-differentiated G1-G2 tumours require surgical resection when possible, while poorly differentiated G3 carcinomas are usually treated with first-line systemic chemotherapy [8, 9]. However, the pathological features of the tumour can only be determined post hoc if the lesion is resected. Therefore, the Ki67 index is usually assessed preoperatively by endoscopic ultrasound fine-needle aspiration. The quantity of material obtained may be small with hemorrhagic alterations, explaining the possible disagreements between Ki67 values on the biopsy and the resected specimen [10, 11]. This is especially true in grade 2 tumours [12, 13]. Therefore, other features, including imaging, would be helpful.

On imaging, tumour size [14] and enhancement have been shown to be helpful to discriminate tumour grades [15–17]. Only a few studies have addressed the value of imaging features for the assessment of pNET, and most of them have focused on tumour enhancement or differential diagnosis with computerized tomography (CT) [16–23]. Manfredi et al recently showed that magnetic resonance (MR) imaging could play a role [15]. Moreover, the apparent diffusion coefficient (ADC) has been shown to be correlated with tumour cellularity and DWI has been shown to be valuable for the detection and characterization of pNETS [24–26], and for the detection of liver metastases [27]. However, there have been very few studies on the added value of DWI for grading tumours [28–30].

The aim of our study was to assess the value of MR including DWI-imaging for the evaluation of tumour grade in a series of resected pNETs.

Methods

Patient population

This retrospective study was approved by the IRB and informed consent was waived. Between 2006 and 2014, 554 resected pNETs were extracted from the local pathological database. Inclusion criteria were the presence of at least one resected pNET and a preoperative contrast-enhanced MR imaging examination including a DWI sequence performed up to 3 months before the resection. At least three b-values were required. Demographic, clinical-biological, and outcome data were retrieved from medical records.

The final population included 94 patients (48 women, 51 %), mean age 52 ± 12 years old (range 29–79) with 108 resected tumours (Fig. 1). The median interval between preoperative MR imaging and resection was 2 months (interquartile range [IQR] 0-9).
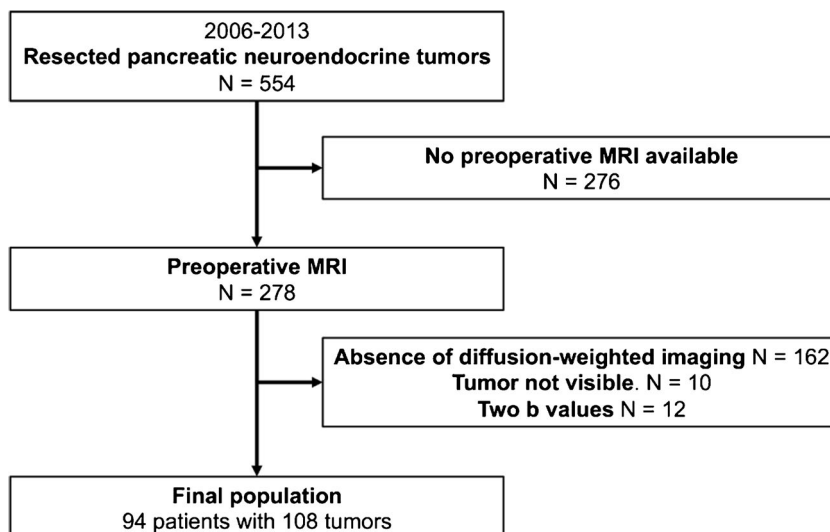
Magnetic resonance imaging

MR imaging was performed with a 1.5-T imager (Intera; Philips Healthcare, Best, the Netherlands) using a phased-array surface coil after 4–6 h of fasting. The protocol (Table 1) included a T2-weighted single-shot sequence, a T2-weighted fast spin-echo sequence with spectral fat saturation, and a transverse breath-hold 3D T1-weighted fat-suppressed spoiled gradient-recalled echo sequence before and after dynamic injection of 0.1 mmol/kg of body weight of gadolinium chelates, followed by a 20-mL saline solution flush at a rate of 2 mL/s administered with a power injector. Pancreatic arterial-dominant, portal venous, and equilibrium phase sequences were performed around 35 s (bolus trigger), 60–70 s, and 180–200 s after intravenous contrast material injection, respectively. A free-breathing, fat-suppressed, single-shot echo planar DW MR sequence was performed before contrast injection with b values of 0, 150, and 600 s/mm^2. Cardiac gating was not used. No antispasmodic drugs were administered.

Image analysis

MR images were retrospectively reviewed by two abdominal radiologists (EL senior resident, and MR with 10 years of experience) on a corresponding workstation (Carestream Health, Rochester, NY, USA). Readers were aware of the diagnosis of NET, but blind to the clinicobiological, and pathological features of patients and tumours.

Qualitative image analysis

Image analysis included the site of the pancreatic tumours, signal intensity on T1-w, T2-w, and DW images compared

Fig. 1 Flow chart for the study population


```
┌─────────────────────────────────────┐
│            2006-2013                 │
│ Resected pancreatic neuroendocrine   │
│              tumors                  │
│              N = 554                 │
└─────────────────────────────────────┘
                  │
                  │───────→ ┌──────────────────────────┐
                  │         │ No preoperative MRI       │
                  │         │ available                 │
                  │         │ N = 276                   │
                  │         └──────────────────────────┘
                  ▼
┌─────────────────────────────────────┐
│         Preoperative MRI             │
│              N = 278                 │
└─────────────────────────────────────┘
                  │
                  │───────→ ┌──────────────────────────────────────┐
                  │         │ Absence of diffusion-weighted imaging │
                  │         │ N = 162                               │
                  │         │ Tumor not visible. N = 10             │
                  │         │ Two b values N = 12                   │
                  │         └──────────────────────────────────────┘
                  ▼
┌─────────────────────────────────────┐
│         Final population             │
│      94 patients with 108 tumors     │
└─────────────────────────────────────┘
```

to the adjacent pancreatic parenchyma (defined as hypo-, iso-, or hyperintense), homogeneity/heterogeneity on T2-w images, cystic components defined as an area of marked T2-w signal intensity similar to that of fluid, dilatation of the main pancreatic duct ≥2.5 mm, dilatation of the bile ducts, arterial or venous encasement, infiltration of peripancreatic fat, contrast enhancement of the tumour on arterial/pancreatic, portal venous, and delayed phase images compared to the adjacent parenchyma (defined as hypo-, iso- or hyperintense), and the presence of lymph nodes >1 cm and liver metastases. The "enhancement pattern" defining a specific combination of the different signal intensities on consecutive arterial and portal venous dynamic phases (i.e. hypo-, iso-, or hyperintensity) was also noted.

Quantitative image analysis

Image analysis included the largest diameter of the tumours on the axial plane and calculation of diffusion-related parameters. Readers were asked to place an ellipsoid region of interest (ROI) on the equatorial plane of each lesion on the intermediate b-value image (b = 150 s/mm^2). The ROI was drawn to include the largest portion of the tumour with no surrounding pancreatic parenchyma and avoiding the cystic components.

ROIs were pasted on the other b-value images. The mean and minimal signal intensity (SI) for each b-value image was noted. The mean and minimal apparent diffusion coefficient (ADC) values and the pure diffusion coefficient (D) values were then calculated using a monoexponential fit (b = 0, 150, and 600 s/mm^2 for ADC and b = 150 and 600 s/mm^2 for D). Similar analysis was performed on the up- and downstream pancreas when possible by placing an ellipsoid ROI on pancreatic parenchyma, avoiding the main pancreatic duct.

Pathology analysis

Haematoxylin and eosin-stained slides of each lesion were retrospectively reviewed by a pancreatic pathologist (JC), blinded to MR imaging data. Tumour differentiation and grading (according to WHO-2010 and ENETS-2012), the presence of angioinvasion and perineural invasion, regional lymph node, and distant metastases and the Ki67 labelling index by the MIB-1 antibody (DAKO, Milano, Italy) were noted. Other subdivisions of the Ki67 index were also used in accordance with recent studies showing an improved evaluation of prognosis (i.e. 0–5 %, 6–15 %, 16–35 %, 36–55 %, and >55 %, or 0–2 %, 3–10 %, >10 %) [1, 6, 7]. Pathological analysis of the adjacent pancreatic parenchyma was also performed.

Table 1 MR sequences parameters

Sequences	N slices	TR/TE (ms)	Slice thickness (mm)	Flip Angle (°)	Matrix size	N Excitations
T2-weighted single-shot sequence	32	890 / 85	5	90	320 x 320	1
T2-weighted fast spin-echo sequence with spectral fat saturation	36	1800 / 90	5	90	352 x 352	1
T1-weighted fat-suppressed spoiled gradient-recalled echo sequence	90	4.6 / 2.2	3	10	240 x 240	2
Diffusion-weighted	32	4033 / 63	6	90	256 x 256	6

Statistical analysis

Results are presented as means (standard deviation) or medians (ranges) for quantitative data, and as the number of cases (percentage of cases) for categorical variables. The comparison between subgroup features was performed with the Student t-test and the Mann–Whitney U test for continuous variables according to distribution. Qualitative data were compared with the Chi2 or Fisher's exact tests when necessary.

In patients with multiple lesions, tumour grades, and Ki67 varied between lesions. Therefore, lesions were considered independent. The diagnostic value of D and ADC for differentiating tumour grades was assessed by receiver operating characteristic (ROC) curve analysis. Curves were compared using the DeLong test, and cut-off values were chosen by maximizing the Youden index. Sensitivity and specificity were computed. Tests were always two sided, and $p < 0.05$ was considered to be significant, except for post-hoc tests, for which $p < 0.017$ was considered to be significant according to the Bonferroni correction. Inter-reader agreement for ADC and D was assessed using a Bland-Altman plot and intraclass correlation coefficient. All analyses were performed

using Statistical Package for the Social Sciences software (version 20.0, IBM SPSS Inc., Armonk, NY, USA).

Results

Patient and tumour characteristics

A total of 94 patients (48 women, 51 %), mean age 52 ± 12 years old, were analysed (Table 2), with 108 tumours (mean 40 ± 33 mm). Eighty-eight patients (94 %) had one lesion, three had two tumours, and the remaining three patients had 3, 4, and 7, respectively. Seventeen patients (18 %) had functioning tumours: gastrinoma (n = 12), insulinoma (n = 3), VIPoma (n = 1), and glucagonoma (n = 1).

At pathology, 55 tumours were classified as G1 (51 %), and 42 (39 %), and 11 (10 %) were classified as G2, and G3, respectively. Size increased with grade (26 ± 17, 47 ± 34, and 86 ± 52 mm for G1, G2, and G3, respectively, $p < 0.001$, with a significant correlation between size and Ki67: r = 0.54, $p < 0.001$). Among G3 tumours, five (45 %) were poorly differentiated. These lesions were larger than differentiated G3

Table 2 Patients and tumours characteristics

	Overall (N = 108)	G1 (N = 55)	G2 (N = 42)	G3 (N = 11)	*p*-value
Patients characteristics (n = 94)					
M/F (%)	43/46	16/29 (36/64)	22/16 (58/42)	8/3 (73/27)	**0.031**
Mean age ± SD	52 ± 12	51 ± 10	53 ± 13	55 ± 17	0.479
Medical history					
None	83 (77)	36 (65)	36 (86)	11 (100)	
Multiple endocrine neoplasia type 1	8 (8)	7 (13)	1 (2)	0 (-)	
Tuberous sclerosis	1 (1)	1 (2)	0 (-)	0 (-)	**0.010**
Von-Hippel-Lindau	1 (1)	0 (-)	1 (2)	0 (-)	
Autoimmune hepatitis	1 (1)	1 (2)	0 (-)	0 (-)	
Familial history of NET					
Yes (%)	3 (3)	2 (4)	1 (2)	0 (-)	0.783
Tumours features					
Mean size ± SD	40 ± 33	26 ± 17	47 ± 34	86 ± 52	**<0.001**
< 10 mm	8 (7)	6 (11)	2 (5)	0 (-)	
10-19 mm	24 (22)	21 (38)	3 (7)	0 (-)	**<0.001**
20-29 mm	24 (22)	14 (25)	10 (24)	0 (-)	
≥ 30 mm	52 (48)	14 (25)	27 (64)	11 (100)	
Lymph node invasion	24 (22)	6 (11)	9 (21)	9 (82)	**<0.001**
Local invasion	55 (51)	19 (35)	25 (60)	11 (100)	**<0.001**
Ki 67 ± SD	8.2 ± 17.3	1.2 ± 0.37	6.0 ± 3.5	54.0 ± 29.7	**<0.001**
Location					
Head	39 (36)	17 (31)	16 (38)	6 (55)	
Body	36 (33)	22 (40)	12 (29)	2 (18)	0.485
Tail	33 (31)	16 (29)	14 (33)	3 (27)	

NET neuroendocrine tumour. Numbers in brackets are percentages

Table 3 Qualitative MR imaging features

	Overall (N = 108)	G1 (N = 55)	G2 (N = 42)	G3 (N = 11)	*p*-value
Tumour imaging features					
T1-w signal intensity					
Hypo-	90 (83)	47 (85)	34 (81)	9 (82)	
Iso-	17 (16)	8 (15)	7 (17)	2 (18)	0.501
Hyper-	1 (1)	0 (-)	1 (2)	0 (-)	
T2-w signal intensity					
Hypo-	18 (17)	4 (7)	7 (17)	6 (55)	
Iso-	14 (13)	9 (16)	4 (10)	1 (9)	0.578
Hyper-	77 (70)	42 (76)	31 (74)	4 (36)	
Heterogeneity	43 (42)	18 (33)	21 (50)	5 (45)	0.217
Cystic component	23 (22)	18 (33)	4 (10)	1 (9)	**0.011**
Duct dilatation					
Main pancreatic duct	20 (19)	6 (11)	11 (26)	4 (36)	0.055
Biliary tree	6 (6)	1 (2)	5 (12)	1 (9)	0.135
Tumour extension					
Arterial encasement	24 (23)	8 (15)	13 (31)	6 (55)	**0.041**
Venous encasement	24 (23)	6 (11)	14 (33)	6 (55)	**0.002**
Fat invasion	37 (36)	13 (24)	20 (48)	9 (82)	**<0.001**
Lymph nodes	19 (18)	6 (11)	9 (21)	9 (82)	**<0.001**
Liver metastases	29 (28)	9 (16)	15 (36)	8 (73)	**<0.001**
Vascular behavior					
Arterial phase					
Hypo-	13 (12)	3 (5)	3 (7)	7 (63)	
Iso-	18 (17)	8 (15)	6 (14)	4 (36)	**<0.001**
Hyper-	77 (71)	44 (80)	33 (79)	0 (-)	
Portal venous phase					
Hypo-	11 (10)	3 (5)	2 (5)	6 (33)	
Iso-	31 (29)	13 (24)	15 (36)	4 (50)	**<0.001**
Hyper-	65 (60)	39 (80)	25 (60)	1 (17)	
Delayed phase					
Hypo-	13 (12)	4 (7)	4 (10)	5 (17)	
Iso-	33 (31)	16 (29)	13 (31)	4 (50)	**0.005**
Hyper-	62 (57)	35 (64)	25 (60)	2 (33)	
Enhancement pattern on art/port images					
Hyper/iso	13 (12)	5 (9)	8 (19)	0 (-)	0.216
Hyper/hyper	65 (60)	39 (71)	25 (60)	0 (-)	**0.003**
Hypo/hypo	11 (10)	3 (5)	2 (5)	6 (55)	**<0.001**
Hypo/iso	2 (2)	0 (-)	1 (2)	1 (9)	0.118
Iso/iso	16 (15)	8 (15)	5 (12)	4 (36)	0.140
Iso/hyper	1 (1)	0 (-)	1 (2)	0 (-)	0.480
Pancreas					
T1-w signal of downstream pancreas					
Hypo	7 (6)	3 (5)	3 (7)	1 (9)	
Iso	4 (4)	0 (-)	2 (5)	2 (18)	**0.003**
Hyper	80 (74)	48 (87)	29 (60)	3 (27)	
T1-w signal intensity of upstream pancreas					
Hypo	24 (22)	7 (13)	10 (24)	7 (64)	
Iso	0 (-)	0 (-)	0 (-)	0 (-)	**<0.001**
hyper	49 (45)	36 (65)	13 (31)	0 (-)	

Numbers in parentheses are percentages

tumours, but it did not reach the level of significance (109 ± 73 vs. 71 ± 31 mm, $p = 0.279$). They had a higher Ki67 than differentiated G3 tumours (84 ± 11 vs. 34 ± 15, $p < 0.001$).

Qualitative analysis

Arterial/venous encasement ($p = 0.041$ and $p = 0.002$), peritumoural fat invasion, lymph nodes, liver metastases were significantly associated with tumour grade (all $p < 0.001$). Pancreatic duct dilatation was more frequent in G3 tumours (36 % vs. 11 % and 26 % for G1 and G2, respectively), but it did not reach the level of significance ($p = 0.055$) (Table 3).

Most G1-G2 lesions were hypervascular (80 % and 79 % for G1 and G2), while all G3 tumours were hypo/isointense. On portal venous phase images, most G1 lesions were hyper-intense (80 %), while most G3 lesions showed either hypo/isosignal intensity (83 %). All lesions showed signal hyperintensity in b0 and b150, and most lesions (93 %) showed signal hyperintensity on high b-value images.

Several enhancement patterns were observed (Table 3). Hyperintensity on both arterial and portal venous phase images was significantly more frequent in G1 tumours (71 %, vs. 60 % and 0 % for G2 and G3, $p = 0.003$). A combination of hypo/iso (i.e. hypo/hypo, hypo/iso, or iso/iso) was more frequent in G3 lesions (100 % vs. 20 % and 19 % for G1 and G2, $p < 0.001$).

Quantitative analysis

The mean ADC value for the whole cohort was 1.88 ± 0.76 and 1.86 ± 0.70 10^{-3} mm^2/s for readers 1 and 2, respectively (Table 4). The mean D value was 1.80 ± 0.73 and 1.79 ± 0.81 10^{-3} mm^2/s for readers 1 and 2, respectively. Measurements showed significant correlation between readers (r = 0.90 and r = 0.89 for ADC_{mean} and D, both $p < 0.001$). The bias (limits of agreement) between the two readings were -2.7 % (-38 %, +32 %) for ADC_{mean} and +1.3 % (-41 %, +46 %) for D. ICC was 0.90 and 0.87 for ADC and D, respectively.

From this point forward, results are presented for the most experienced reader (reader 1). ADC_{mean} were significantly different among tumour grades, with the lowest values associated with higher-grade tumours ($p < 0.001$, Table 4, Fig. 2). Similar results were observed for the minimum value of ADC (ADC_{min}), and D values ($p < 0.001$ for both, Table 4, Fig. 2). There was a significant correlation between ADC_{mean} and D values (r = 0.91, $p < 0.001$).

Poorly differentiated G3 had significantly lower ADC_{mean} and ADC_{min} values than differentiated G3 tumours (0.69 ± 0.19 vs. 0.97 ± 0.16 10^{-3} mm^2/s, $p = 0.042$, and 0.62 ± 0.23 vs. 0.89 ± 0.14 10^{-3} mm^2/s, $p = 0.044$). D was not significantly different ($p = 0.194$).

There was an inverse correlation between both ADC_{mean} and D values tumour size (r = -0.26, $p = 0.008$ for ADC_{mean} and r = -0.23, $p = 0.02$ for D). There was also an inverse relation between both ADC_{mean} and D values and Ki-67 (for ADC_{mean} r = -0.55, for D r = -0.41, both $p < 0.001$). When tumours were grouped according to different Ki-67 classes

Table 4 Diffusion-weighted MR imaging parameters

	Overall (N = 108)	G1 (N = 55)	G2 (N = 42)	G3 (N = 11)	*p*-value
Tumour					
$ADC_{mean} \pm SD$ Reader 1	1.88 ± 0.76	2.13 ± 0.70	1.78 ± 0.72	0.86 ± 0.22	**<0.001**
$D_{mean} \pm SD$ Reader 1	1.80 ± 0.73	1.92 ± 0.70	1.75 ± 0.74	0.82 ± 0.19	**<0.001**
$ADC_{mean} \pm SD$ Reader 2	1.86 ± 0.70	2.15 ± 0.66	1.67 ± 0.57	1.00 ± 0.42	**<0.001**
$D_{mean} \pm SD$ Reader 2	1.79 ± 0.81	1.91 ± 0.72	1.77 ± 0.70	0.92 ± 0.17	**<0.001**
$ADC_{min} \pm SD$	1.40 ± 0.56	1.52 ± 0.59	1.33 ± 0.49	0.78 ± 0.22	**<0.001**
Downstream pancreas					
$ACD_{mean} \pm SD$	1.92 ± 0.69	1.96 ± 0.77	1.85 ± 0.57	1.77 ± 0.69	0.723
$D_{mean} \pm SD$	1.53 ± 0.49	1.52 ± 0.53	1.54 ± 0.38	1.60 ± 0.78	0.949
Upstream pancreas					
$ADC_{mean} \pm SD$	2.96 ± 0.86	2.98 ± 0.89	3.15 ± 0.52	2.41 ± 0.13	0.485
$D_{mean} \pm SD$	1.44 ± 0.51	1.41 ± 0.55	1.50 ± 0.48	1.48 ± 0.47	0.769

ADC and D are expressed in 10^{-3} mm^2/s

ADC_{mean} values were significantly different among tumour grades (G1 vs. G2 $p = 0.038$, G2 vs. G3 $p < 0.001$ and G1 vs. G3 $p < 0.001$).

D values did not significantly differ between G1 and G2 tumours ($p = 0.802$), but were significantly lower in G3 tumours (vs. G1 $p < 0.001$ and vs. G2 $p = 0.001$).
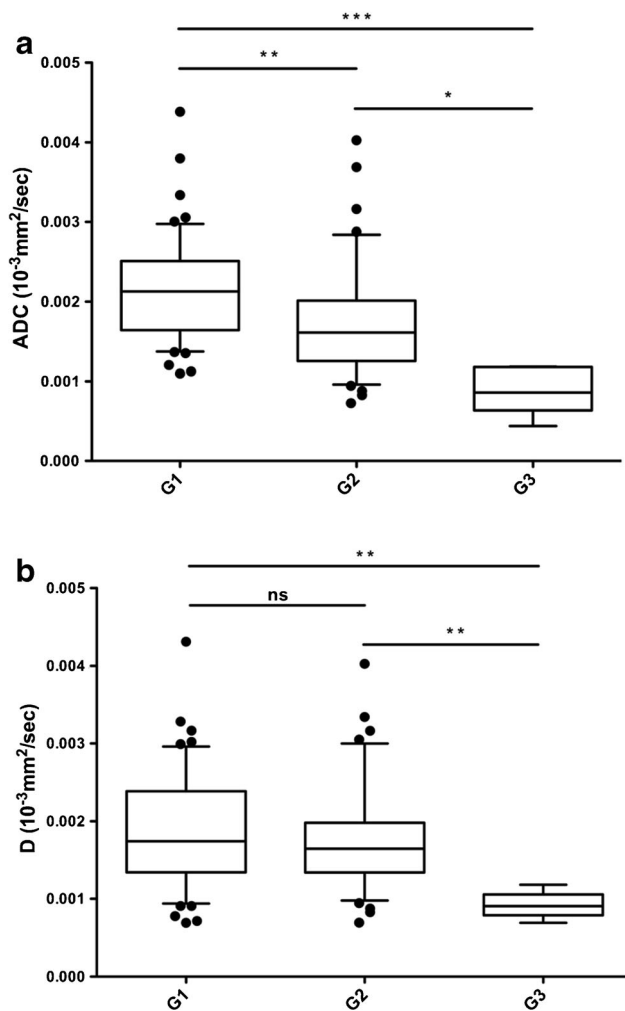
Fig. 2 Distribution of the ADC_{mean} (**a**), ADC_{min}, (**b**), and D (**c**) values according to the tumour grade. ADC and D values were significantly lower in higher tumour grades ($p < 0.001$, for all). * $p < 0.05$, ** $p < 0.01$, *** $p < 0.001$

following recent publications (0–5 %, 6–15 %, 16–35 %, 36–55 %, >55 %) there was a significant and gradual decrease in both ADC_{mean} and D values ($p < 0.001$ for both, Table 5, Fig. 3). When dividing G2 tumours according to the Ki-67 (3–10 % and 11–20 %), ADC_{mean} and D both significantly decreased ($p < 0.001$ and $p = 0.0008$ for ADC_{mean}, and D,

respectively, Table 5, Fig. 3). Comparison with the pancreatic parenchyma is provided as supplemental material.

Prediction of tumour grade

The sensitivity and specificity of the different qualitative morphological features for the identification of G3 tumours (vs. G1-2) ranged from 36 % to 100 %, and 33 % to 95 %, respectively, with AUROCs ranging from 0.49 to 0.90 (Table 6). ADC_{mean} and D showed the largest AUROC (0.96 and 0.95, respectively, $p > 0.05$, Fig. 4). ADC_{min} had an AUROC of 0.83 (vs. ADC_{mean} $p = 0.04$, and vs. D $p = 0.06$). Optimal cut-off values for ADC_{mean} and D for the identification of G3 lesions were 1.19 10^{-3} mm²/s (sensitivity 100 %, specificity 92 %), and 1.04 10^{-3} mm²/s (sensitivity 83 %, specificity 92 %) (Fig. 5).

Qualitative morphological features were less sensitive and specific for the identification of G1 tumours (vs. G2-3) (Supplemental Figure 1). Sensitivity ranged from 49 % to 95 %, and specificity from 15 % to 91 %, with the AUROC ranging from 0.52 to 0.73 (Table 6). AUROCs for ADC_{mean}, ADC_{min} and D were 0.75, 0.75, and 0.66, respectively (all comparisons $p > 0.05$, Fig. 4). Supplemental Figure 2 provides a combination of morphological and functional imaging features for the stratification of tumour grades.

Discussion

The present study shows that morphological and functional MR findings, including DWI, have predictive value for pNET tumour grade, especially for the differentiation between G3 and G1-2 tumours.

For the prediction of tumour grade has been shown to be strongly associated with size [14]. Thus, proliferation in small lesions is more likely to be low. This explains results in previous studies showing that incidentally identified non-functioning lesions <2 cm can be managed by active surveillance, because the risk of malignancy and distant progression is very low [31–33]. This was also true in the present study as

Table 5 Diffusion-weighted MR parameters according to alternative Ki-67 thresholds

All lesions	0-5 % (N = 77)	6-15 % (N = 19)	16-35 % (N = 4)	36-55 % (N = 1)	>55 % (N = 2)	p-value
$ADC_{mean} \pm SD$	2.13 ± 0.70	1.51 ± 0.50	1.08 ± 0.16	0.88	0.72 ± 0.17	**<0.001**
$D_{mean} \pm SD$	1.95 ± 0.74	1.50 ± 0.50	1.11 ± 0.19	0.82	0.70 ± 0.18	**<0.001**
G1-G2 group	0-2 % (N = 55)	3-10 % (N = 37)	11-20 % (N = 5)			p-value
$ADC_{mean} \pm SD$	2.17 ± 0.66	1.78 ± 0.72	0.90 ± 0.27			**<0.001**
$D_{mean} \pm SD$	1.91 ± 0.71	1.76 ± 0.74	0.92 ± 0.17			**0.0008**

ADC and D are expressed in 10^{-3} mm²/s

Fig. 3 Distribution of the ADC$_{mean}$ (**a**) and D (**b**) values according to the tumour Ki-67. ADC$_{mean}$ and D values were significantly lower in higher tumour grades ($p < 0.001$ for both). Distribution of the ADC$_{mean}$ (**c**) and D (**d**) values according to the Ki-67 of G1 and G2 lesion. ADC$_{mean}$ and D values were significantly lower as Ki-67 increased ($p < 0.001$ for both)
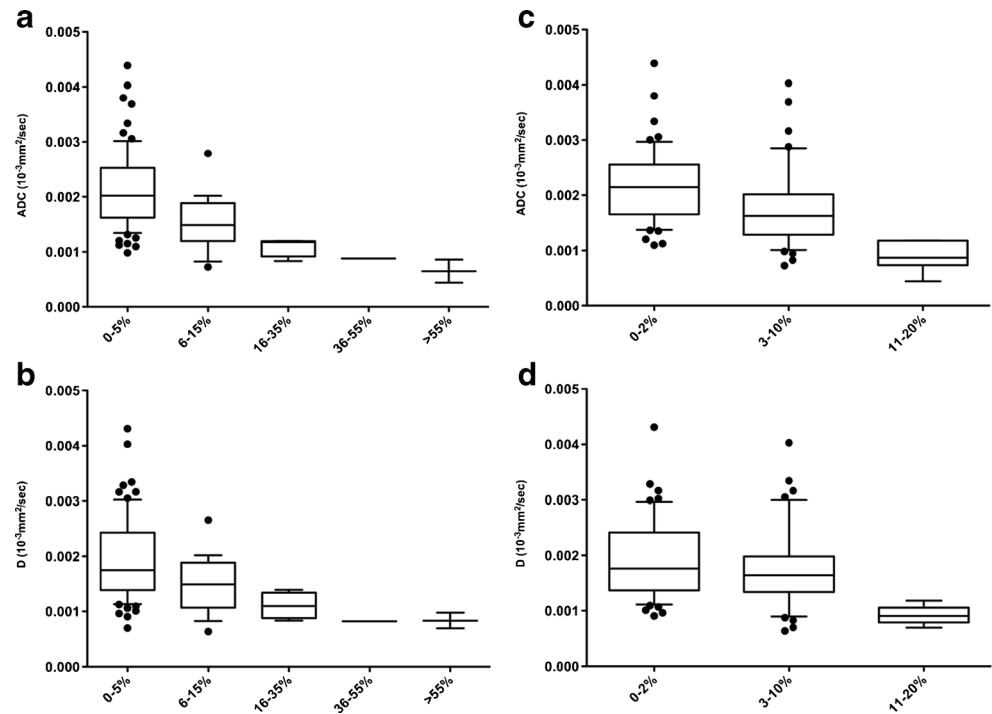
all G3 lesions were >3 cm, and 75 % of <10 mm were G1, with significant correlation between tumour size and Ki67. This has also been reported in other series evaluating imaging features with MR [15, 34] or CT [16, 19, 35].

Nevertheless, size alone is insufficient for the accurate discrimination of tumour grade, especially between G1 and G2 tumours. Moreover, small lesions may be aggressive [36]. Therefore, numerous other imaging features have been described including vascular invasion or the presence of regional lymph nodes [15, 19].

One important feature that is classically associated with pNET is hypervascularity. Studies have shown that tumour enhancement on CT is correlated with tumour vascularity on light microscopy, and that low-enhancing NETs are poorly differentiated and show decrease overall survival [20, 35]. In the present series, most G1, and to a lesser extent, G2 lesions were hypervascular, while no G3 showed this feature. Recently, Capelli et al suggested that in addition to evaluating tumour enhancement during the arterial phase the tumour enhancement pattern during portal venous and delayed phases might also provide information [16]. This study showed that tumours with significant delayed enhancement alone were often neuroendocrine carcinomas. Our results do not support these observations. If most G3 lesions were hypo- or isointense on both arterial and portal venous phase images, 33 % of these tumours were hyperintense on delayed phase images, but this was not specific to G3 tumours. This may be

partially explained by the different imaging modalities, because Capelli et al used contrast-enhanced CT [16].

There was an inverse relationship between ADC and D and tumour size, but one important result of this study is the stronger significant and negative relationship between ADC and D and the degree of tumour proliferation. This supports previous studies by Wang et al. and Jang et al. [28, 29]. Interestingly, in the present study, both ADC and D were significantly and negatively correlated with Ki67 labelling. Our results differ from the study by Hwang et al with IVIM that did not find any difference in ADC values between G1 and G2-3 lesions [34]. Because low grade NETs are hypervascular, perfusion plays a significant role in tumour behaviour and characterization [37]. D'Assignies et al showed that perfusion CT values are correlated with histoprognostic factors, such as the proliferation index and the WHO classification [18]. Thus, the parameter D, which reflects pure water diffusion, could be expected to be less discriminatory for tumour grade than ADC. In fact, the AUROCs for the differentiation between G3 and G1-2 lesions for ADC and D were similar. The difference between our results and those by Hwang et al may be due to the inclusion of fewer pNETs in their study (40 tumours with only one G3 tumour).

We also analyzed the performance of the minimum ADC value as previous studies have reported a significant correlation with Ki67 in other tumours [38, 39]. As expected, ADC$_{min}$ decreased as the tumour grade and the Ki67

Table 6 Diagnostic performances of clinical and imaging features

G3 vs. 1-2	AUROC ± SD	Sensitivity (%)	Specificity (%)
Male gender	0.64 ± 0.09	73	54
Tumour size ≥ 20 mm	0.70 ± 0.08	100	33
Tumour size ≥ 30 mm	0.77 ± 0.06	100	58
MPD dilatation	0.56 ± 0.11	36	82
Arterial encasement	0.49 ± 0.10	55	78
Venous encasement	0.61 ± 0.11	55	79
Fat invasion	0.76 ± 0.07	82	68
Lymph nodes	**0.87 ± 0.07**	82	85
Metastases	0.78 ± 0.07	73	75
Non hypervascular on arterial phase	**0.90 ± 0.03**	100	79
Non hypervascular on portal phase	0.78 ± 0.06	83	66
Non Hyper/hyper	0.75 ± 0.10	100	34
Hypo/hypo	**0.81 ± 0.10**	55	95
ADC mean	**0.96 ± 0.02**		
ADC min	**0.83 ± 0.06**		
D	**0.95 ± 0.02**		
G1 vs. 2-3	AUROC ± SD	Sensitivity (%)	Specificity (%)
Female gender	0.63 ± 0.06	53	61
Tumour size < 20 mm	0.72 ± 0.06	49	91
Tumour size < 30 mm	0.73 ± 0.05	75	72
No MPD dilatation	0.58 ± 0.06	89	28
No arterial encasement	0.59 ± 0.06	85	36
No venous encasement	0.63 ± 0.06	89	38
No fat invasion	0.69 ± 0.06	76	55
No lymph nodes	0.62 ± 0.06	89	34
No metastases	0.68 ± 0.06	84	43
Hypervascular on arterial phase	0.56 ± 0.06	80	38
Hypervascular on portal phase	0.58 ± 0.06	80	51
Hyper/hyper	0.58 ± 0.06	71	53
Non Hypo/hypo	0.52 ± 0.06	95	15
ADC mean	0.75 ± 0.05		
ADC min	0.65 ± 0.05		
D	0.66 ± 0.05		

AUROCs ≥ 0.80 are bold; *MPD* main pancreatic duct

increased, but with lower performance that that of ADC_{mean}. Further studies are necessary to validate these results.

Size and ADC values helped identify G1 and G2 tumours among hypervascular lesions, although the predictive value was lower. Indeed, even if the ADC and D values in our study were found to be significantly different for the three tumour grades, the AUROC of ADC and D were lower for the differentiation between G1 and G2, and there was significant overlap between these two groups. This is partially explained by the small range of Ki67 labelling for G1, and a wider range for G2 tumours [2]. Recently, authors have shown that modified Ki67 thresholds provide a clinically effective prognostic stratification of patients [1, 6, 7]. While waiting for possible revision of this classification, we also applied these modified thresholds (i.e. 0–5 %, 6–15 %, 15–35 %, 36–55 %, >55 %) and observed a more gradual decrease in both ADC and D values, and better discrimination of lesions with low Ki67 labelling.

Finally, the ADC and D values of the pancreatic parenchyma could not help predict tumour grade. Yet, and even though it was not the main objective of the present study, ADC and D of the tumours were significantly lower than those of the upstream pancreas in all grades, and of that of the downstream pancreas in high-grade tumours. This might help differentiate
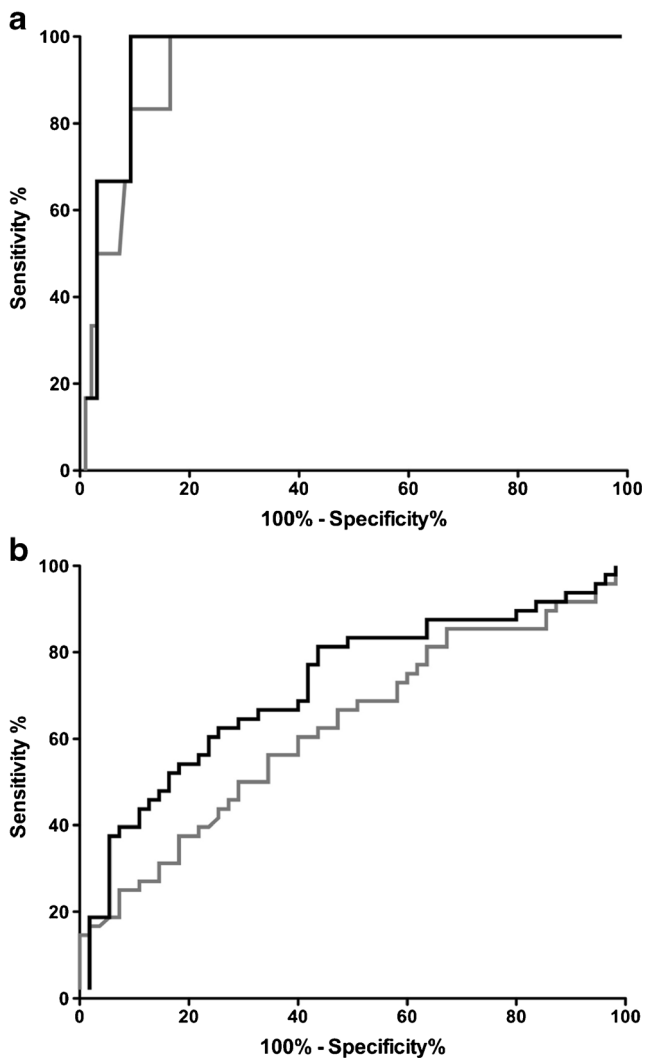
Fig. 4 ROC curves of ADC$_{mean}$ (*black lines*), ADC$_{min}$ (*thin black line*), and D (*grey lines*) for the differentiation between G1-2 and G3 tumours (**a**), and between G1 and G2-3 tumours (**b**)
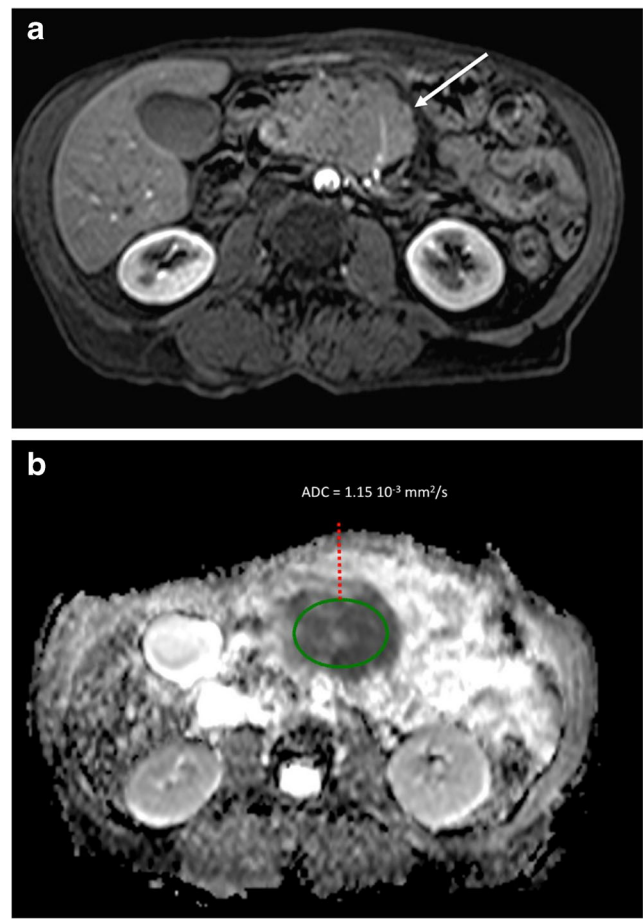

Fig. 5 Example of a G3 pNET of the body of the pancreas in a 66 year old woman. MR imaging showed a large (>2 cm) non-hypervascular lobulated tumour on arterial phase images (*arrow* in **a**) with a mean ADC value of 1.15 10^{-3} mm^2/s (**b**). All features were consistent with a G3 tumour. The lesion was resected, and pathological analysis confirmed the tumour grade (Ki67 = 25 %)

tumours from the pancreatic parenchyma in difficult cases. This statement requires further validation.

Besides its retrospective design, our study has certain limitations. First, there were fewer G3 tumours than G1 and G2 tumours. This was partially due to our selection process, as we only included patients with resected lesions. Another part of the explanation is that G3 tumours are less frequent than G1-2 tumours (around 11 % in a series of more than 35,000 patients [40]). Therefore, our population can be reasonably considered as representative of the distribution of pNETs in the general population. Finally and importantly, inclusion of patients undergoing biopsy rather than resection would expose to a risk of misclassification as biopsy may be subject to variability and error. Second, we did not analyse the outcome of the patients,

and the influence of diffusion parameters on survival or recurrence.

In conclusion, the combination of morphological and functional MR imaging features is useful for the discrimination of tumour grade in pNETS. Diffusion imaging parameters are significantly associated with tumour proliferation, and helpful for the identification of high-grade and poorly differentiated tumours.

References

1. Zerbi A, Falconi M, Rindi G et al (2010) Clinicopathological features of pancreatic endocrine tumors: a prospective multicenter study in Italy of 297 sporadic cases. Am J Gastroenterol 105:1421–1429

2. Kloppel G (2011) Classification and pathology of gastroenteropancreatic neuroendocrine neoplasms. Endocr-Relat Cancer 18:S1–S16

3. Klimstra DS, Modlin IR, Coppola D, Lloyd RV, Suster S (2010) The pathologic classification of neuroendocrine tumors: a review of nomenclature, grading, and staging systems. Pancreas 39:707–712

4. Kloppel G, Rindi G, Perren A, Komminoth P, Klimstra DS (2010) The ENETS and AJCC/UICC TNM classifications of the neuroendocrine tumors of the gastrointestinal tract and the pancreas: a statement. Virchows Arch Int J Pathol 456:595–597

5. Plockinger U, Rindi G, Arnold R et al (2004) Guidelines for the diagnosis and treatment of neuroendocrine gastrointestinal tumours. A consensus statement on behalf of the European Neuroendocrine Tumour Society (ENETS). Neuroendocrinology 80:394–424

6. Scarpa A, Mantovani W, Capelli P et al (2010) Pancreatic endocrine tumors: improved TNM staging and histopathological grading permit a clinically efficient prognostic stratification of patients. Mod Pathol 23:824–833

7. Bettini R, Boninsegna L, Mantovani W et al (2008) Prognostic factors at diagnosis and value of WHO classification in a mono-institutional series of 180 non-functioning pancreatic endocrine tumours. Ann Oncol 19:903–908

8. Ramage JK, Ahmed A, Ardill J et al (2012) Guidelines for the management of gastroenteropancreatic neuroendocrine (including carcinoid) tumours (NETs). Gut 61:6–32

9. Bilimoria KY, Tomlinson JS, Merkow RP et al (2007) Clinicopathologic features and treatment trends of pancreatic neuroendocrine tumors: analysis of 9,821 patients. J Gastrointest Surg 11:1460–1467, **discussion 1467–1469**

10. Alexiev BA, Darwin PE, Goloubeva O, Ioffe OB (2009) Proliferative rate in endoscopic ultrasound fine-needle aspiration of pancreatic endocrine tumors: correlation with clinical behavior. Cancer 117:40–45

11. Rebours V, Cordova J, Couvelard A et al (2015) Can pancreatic neuroendocrine tumour biopsy accurately determine pathological characteristics? Dig Liver Dis. doi:10.1016/j.dld.2015.06.005

12. Weynand B, Borbath I, Bernard V et al (2014) Pancreatic neuroendocrine tumour grading on endoscopic ultrasound-guided fine needle aspiration: high reproducibility and inter-observer agreement of the Ki-67 labelling index. Cytopathol Off J Br Soc Clin Cytol 25:389–395

13. Hasegawa T, Yamao K, Hijioka S et al (2014) Evaluation of Ki-67 index in EUS-FNA specimens for the assessment of malignancy risk in pancreatic neuroendocrine tumors. Endoscopy 46:32–38

14. Bettini R, Partelli S, Boninsegna L et al (2011) Tumor size correlates with malignancy in nonfunctioning pancreatic endocrine tumor. Surgery 150:75–82

15. Manfredi R, Bonatti M, Mantovani W et al (2013) Non-hyperfunctioning neuroendocrine tumours of the pancreas: MR imaging appearance and correlation with their biological behaviour. Eur Radiol 23:3029–3039

16. Cappelli C, Boggi U, Mazzeo S et al (2015) Contrast enhancement pattern on multidetector CT predicts malignancy in pancreatic endocrine tumours. Eur Radiol 25:751–759

17. Koito K, Namieno T, Nagakawa T, Morita K (1997) Delayed enhancement of islet cell carcinoma on dynamic computed tomography: a sign of its malignancy. Abdom Imaging 22:304–306

18. d'Assignies G, Couvelard A, Bahrami S et al (2009) Pancreatic endocrine tumors: tumor blood flow assessed with perfusion CT reflects angiogenesis and correlates with prognostic factors. Radiology 250:407–416

19. Kim DW, Kim HJ, Kim KW et al (2015) Neuroendocrine neoplasms of the pancreas at dynamic enhanced CT: comparison between grade 3 neuroendocrine carcinoma and grade 1/2 neuroendocrine tumour. Eur Radiol 25:1375–1383

20. Rodallec M, Vilgrain V, Couvelard A et al (2006) Endocrine pancreatic tumours and helical CT: contrast enhancement is correlated with microvascular density, histoprognostic factors and survival. Pancreatology 6:77–85

21. Kim DW, Kim HJ, Kim KW et al (2016) Prognostic value of CT findings to predict survival outcomes in patients with pancreatic neuroendocrine neoplasms: a single institutional study of 161 patients. Eur Radiol 26:1320–1329

22. Kim JH, Eun HW, Kim YJ, Lee JM, Han JK, Choi BI (2016) Pancreatic neuroendocrine tumour (PNET): Staging accuracy of MDCT and its diagnostic performance for the differentiation of PNET with uncommon CT findings from pancreatic adenocarcinoma. Eur Radiol 26:1338–1347

23. Park HS, Kim SY, Hong SM et al (2016) Hypervascular solid-appearing serous cystic neoplasms of the pancreas: differential diagnosis with neuroendocrine tumours. Eur Radiol 26:1348–1358

24. Barral M, Sebbag-Sfez D, Hoeffel C et al (2013) Characterization of focal pancreatic lesions using normalized apparent diffusion coefficient at 1.5-Tesla: preliminary experience. Diagn Interv Imaging 94:619–627

25. Kang KM, Lee JM, Yoon JH, Kiefer B, Han JK, Choi BI (2014) Intravoxel incoherent motion diffusion-weighted MR imaging for characterization of focal pancreatic lesions. Radiology 270:444–453

26. Brenner R, Metens T, Bali M, Demetter P, Matos C (2012) Pancreatic neuroendocrine tumor: added value of fusion of T2-weighted imaging and high b-value diffusion-weighted imaging for tumor detection. Eur J Radiol 81:e746–e749

27. d'Assignies G, Fina P, Bruno O et al (2013) High sensitivity of diffusion-weighted MR imaging for the detection of liver metastases from neuroendocrine tumors: comparison with T2-weighted and dynamic gadolinium-enhanced MR imaging. Radiology 268:390–399

28. Wang Y, Chen ZE, Yaghmai V et al (2011) Diffusion-weighted MR imaging in pancreatic endocrine tumors correlated with histopathologic characteristics. J Magn Reson Imaging 33:1071–1079

29. Jang KM, Kim SH, Lee SJ, Choi D (2014) The value of gadoxetic acid-enhanced and diffusion-weighted MRI for prediction of grading of pancreatic neuroendocrine tumors. Acta Radiol 55:140–148

30. Pereira JA, Rosado E, Bali M, Metens T, Chao SL (2015) Pancreatic neuroendocrine tumors: correlation between histogram analysis of apparent diffusion coefficient maps and tumor grade. Abdom Imaging 40:3122–3128

31. Birnbaum DJ, Gaujoux S, Cherif R et al (2014) Sporadic nonfunctioning pancreatic neuroendocrine tumors: prognostic significance of incidental diagnosis. Surgery 155:13–21

32. Gaujoux S, Partelli S, Maire F et al (2013) Observational study of natural history of small sporadic nonfunctioning pancreatic neuroendocrine tumors. J Clin Endocrinol Metab 98:4784–4789

33. Kishi Y, Shimada K, Nara S, Esaki M, Hiraoka N, Kosuge T (2014) Basing treatment strategy for non-functional pancreatic neuroendocrine tumors on tumor size. Ann Surg Oncol 21:2882–2888

34. Hwang EJ, Lee JM, Yoon JH et al (2014) Intravoxel incoherent motion diffusion-weighted imaging of pancreatic neuroendocrine tumors: prediction of the histologic grade using pure diffusion coefficient and tumor size. Invest Radiol 49: 396–402

35. Luo Y, Dong Z, Chen J et al (2014) Pancreatic neuroendocrine tumours: correlation between MSCT features and pathological classification. Eur Radiol 24:2945–2952

36. Gratian L, Pura J, Dinan M, Roman S, Reed S, Sosa JA (2014) Impact of extent of surgery on survival in patients with small non-functional pancreatic neuroendocrine tumors in the United States. Ann Surg Oncol 21:3515–3521

37. Klau M, Mayer P, Bergmann F et al (2015) Correlation of histological vessel characteristics and diffusion-weighted imaging intravoxel incoherent motion-derived parameters in pancreatic ductal adenocarcinomas and pancreatic neuroendocrine tumors. Invest Radiol 50:792–797

38. Surov A, Caysa H, Wienke A, Spielmann RP, Fiedler E (2015) Correlation between different ADC fractions, cell count, Ki-67, total nucleic areas and average nucleic areas in meningothelial meningiomas. Anticancer Res 35:6841–6846

39. Karaman A, Durur-Subasi I, Alper F et al (2015) Correlation of diffusion MRI with the Ki-67 index in non-small cell lung cancer. Radiol Oncol 49:250–255

40. Yao JC, Hassan M, Phan A et al (2008) One hundred years after "carcinoid": epidemiology of and prognostic factors for neuroendocrine tumors in 35,825 cases in the United States. J Clin Oncol 26:3063–3072